



## Room Temperature Deformation-induced Solute Segregation and its Impact on Twin Boundary Mobility in a Mg-Y Alloy

Xin Wang<sup>a,\*</sup>, Yang Hu<sup>a</sup>, Kehang Yu<sup>a</sup>, Subhash Mahajan<sup>b</sup>, Irene J. Beyerlein<sup>c</sup>, Enrique J. Lavernia<sup>a</sup>, Timothy J. Rupert<sup>a</sup>, Julie M. Schoenung<sup>a</sup>

<sup>a</sup> Department of Materials Science and Engineering, University of California, Irvine, CA, USA

<sup>b</sup> Department of Materials Science and Engineering, University of California, Davis, CA, USA

<sup>c</sup> Mechanical Engineering Department, Materials Department, University of California, Santa Barbara, CA, USA

### ARTICLE INFO

#### Article history:

Received 15 January 2021

Revised 3 September 2021

Accepted 25 October 2021

#### Keywords:

Twinning

Basal-prismatic facet

Solute segregation

HAADF-STEM

Molecular dynamics

### ABSTRACT

Mechanical behavior of alloys is influenced by segregation of solute atoms, which affects deformation mechanisms, such as slip and twinning. In this study, we report on an atomic-scale investigation into room temperature, deformation-induced solute segregation in a Mg-Y alloy. High concentrations of Y were observed at the dislocation cores. In addition, we found that  $\{10\bar{1}2\}$  twins were bounded by coherent twin boundaries and basal-prismatic facets, which contained periodic segregation of Y-rich columns and nano-sized Y-rich clusters, respectively. The observed segregation arrangement was energetically attributed to the fact that it minimizes the overall lattice distortion and is kinetically assisted by the dynamic interaction between solute atoms and crystallographic defects and the slip-twin interaction during plastic deformation. Moreover, segregated Y atoms exert a pinning effect and lead to anisotropy on the mobility of twin boundaries. This finding offers a potentially new alloy design path to control the mechanical response of Mg alloys.

© 2021 Acta Materialia Inc. Published by Elsevier Ltd. All rights reserved.

The discovery of new materials to meet the ever-changing industrial demands is often achieved through alloying. In the past few decades, this effort has been extensively applied to Mg, which holds significant potential for lightweight structural applications. Because of its hexagonal close packed crystal structure, Mg has inherent plastic anisotropy, typically leading to insufficient room temperature formability. The active slip modes in Mg are largely confined to its close-packed basal planes, without easy slip systems to accommodate deformation in the  $\langle c \rangle$  direction [1–6].  $\{10\bar{1}2\}$  twinning can be activated to accommodate strain along  $\langle c \rangle$ -axis tension, making it an important deformation mechanism in Mg in addition to dislocation slip [7–9]. It has been well documented that the addition of alloying elements, particularly dilute concentrations of rare earth elements, such as Y [10–15] or Ce [16,17], can dramatically weaken the crystallographic texture and simultaneously improve the formability and strength of Mg. Such an effect has been attributed to the influence of solute atoms on the flow stresses and relative activities of different slip and twinning modes. Elucidating the fundamental mechanisms by which alloying elements

affect slip and twinning is critical for the design of new advanced Mg alloys.

One important question concerns the spatial distribution of alloying elements. Most studies modeling solute strengthening in Mg include assumptions that the alloying addition stay in solution and are randomly distributed in dilute alloys without considering the potential for rearrangement during plastic deformation [18–20], although the diffusion of solute atoms to the elastic strain field of dislocations, a phenomenon known as strain aging, has been reported in a wide range of material systems [21–23]. Besides dislocations, high-angle annular dark-field scanning transmission electron microscopy (HAADF-STEM) results have demonstrated that solute atoms, e.g., Gd, Ag, Zn and Al, can segregate on coherent twin boundaries (CTBs) in Mg alloys after annealing [24–28]. Such segregation increases the thermal stability and hinders the motion of CTBs [24,27]. However, compared to solute segregation observed after annealing, deformation-induced TB segregation at room temperature [29] and its impact on the mechanical behavior and microstructural evolution of Mg alloys have not been explored. Moreover, both experimental [30–32] and simulation [31–36] studies have demonstrated the potential importance of basal-prismatic (BP) facets on  $\{10\bar{1}2\}$  twin boundaries (TBs) during twin growth; however, segregation of solute atoms to such facets and its impact on the energetics associated with  $\{10\bar{1}2\}$  TB migration

\* Corresponding author: University of California, Irvine, 544 Engineer Tower, Irvine, CA 92617, United States.

E-mail address: [xinw15@uci.edu](mailto:xinw15@uci.edu) (X. Wang).

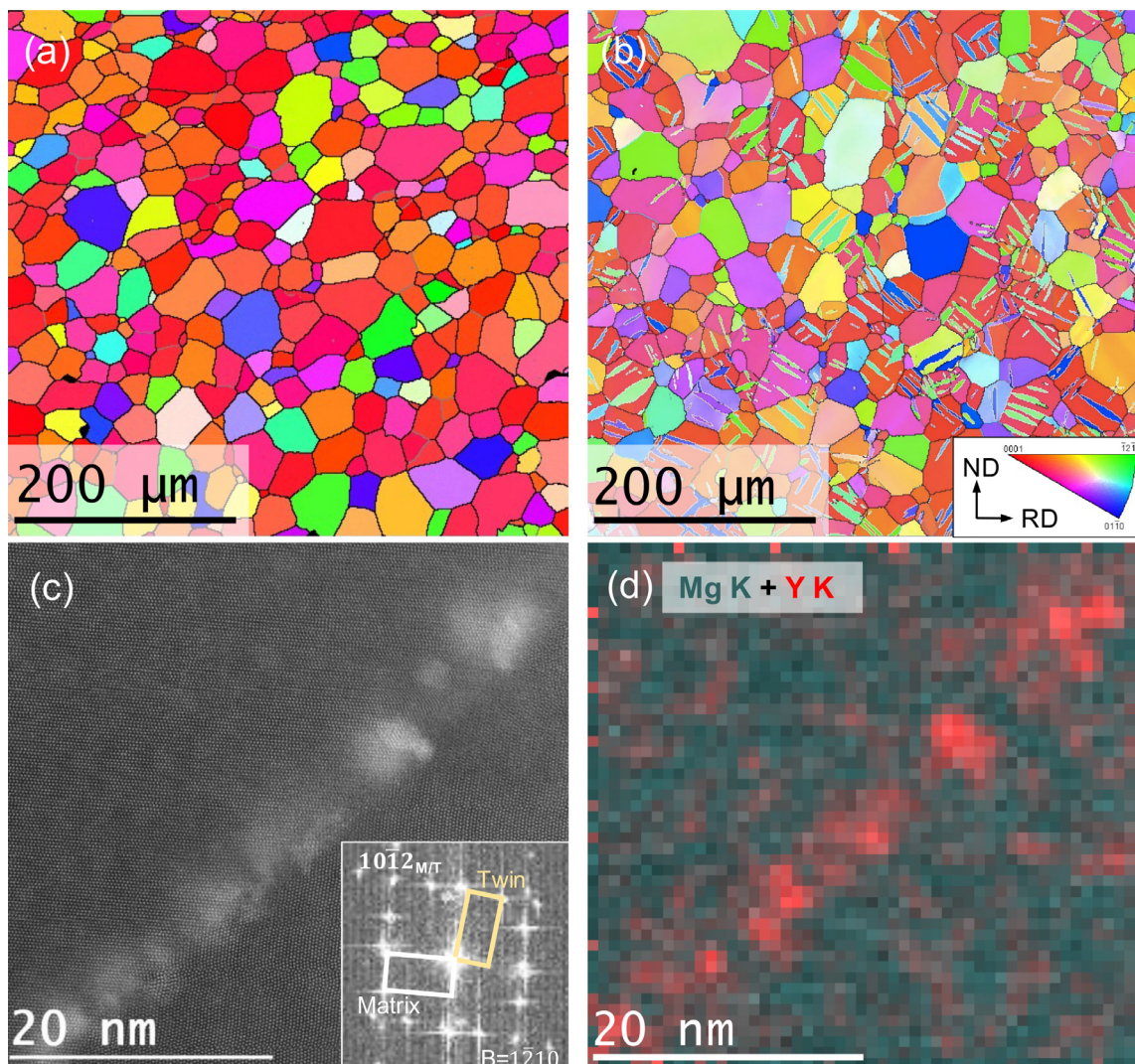
have not been investigated. To address this lack of understanding, we report on the segregation of solute atoms to dislocations and faceted  $\{10\bar{1}2\}$  TBs, composed of CTBs and BP facets, in a Mg-Y binary alloy that has been deformed at room temperature without subsequent annealing. High-resolution STEM and atomistic modeling were combined to investigate the distribution and pinning effects of segregated Y atoms, shedding light on a mechanism by which alloying affect the subsequent mechanical behavior of Mg.

The starting material is a pre-rolled and fully recrystallized single-phase Mg-3 wt.% Y (Mg-3Y) alloy, provided by Helmholtz-Zentrum Geetchacht, Germany. The alloys were cast with high-purity Mg and pure Y, as described in previous studies using similar materials [37,38]. The sample was sectioned into  $4 \times 4 \times 6$  mm cuboids and quasi-statically compressed at room temperature along the rolling direction (RD) to  $\sim 2\%$  plastic strain. Energy dispersive X-ray spectroscopy (EDS) and electron backscattered diffraction (EBSD) were performed using a Tescan GAIA3 scanning electron microscope, equipped with an Oxford AZtecEnergy Advanced EDS System and an AztecHLK NordlysMax2 EBSD system. EDS of the starting material (Fig. S1(a)) estimates the weight percent of Y is approximately 3 wt.%, which is consistent with its nominal composition. EBSD maps show the starting material (Fig. 1(a)) has equiaxed grains with an average size of  $\sim 26 \mu\text{m}$

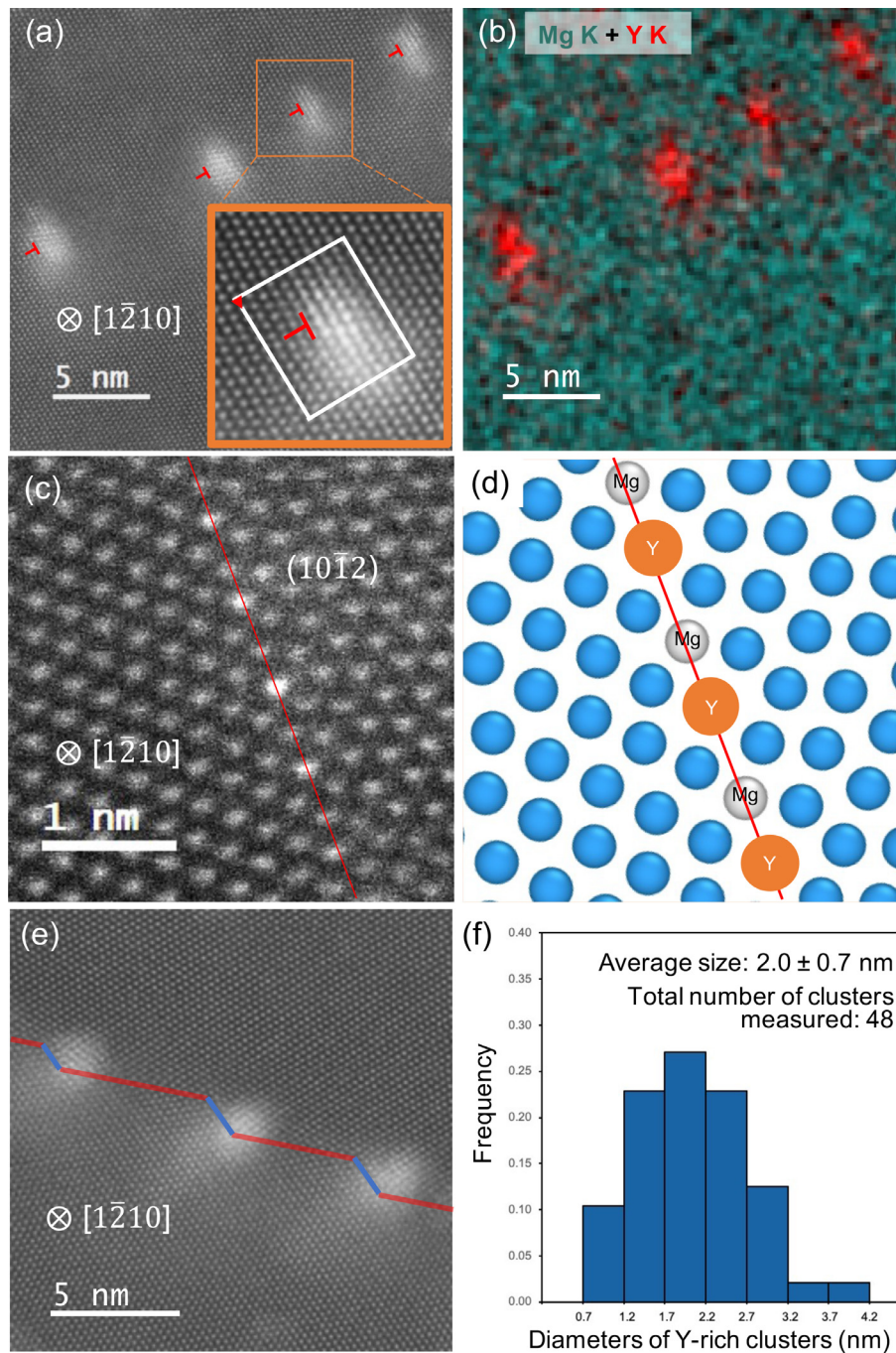
and is free of twins, while profuse newly formed lenticular-shaped  $\{10\bar{1}2\}$  twins were observed after compression (Fig. 1(b)), with a twin area fraction of  $\sim 9.2\%$ . To prepare specimens for STEM observation, the compressed Mg-3Y was sectioned parallel to the RD, mechanically-polished and chemically-etched by a Nital solution. The thin foils were ion milled to electron transparency at cryogenic temperature. A double aberration-corrected JEOL JEM-ARM300F TEM operated at 300 kV was used for microstructure and chemical analyses. For HAADF-STEM imaging, a 35 pA probe current and 6 cm camera length were used, with the inner and outer collection angles being 106 and 180 mrad, respectively.

Fig. S1(b) shows a representative HAADF-STEM image of the undeformed Mg-3Y sample. No Y-rich nanoclusters exist in the starting material. Fig. 1(c) shows an annular dark field (ADF)-STEM image of a representative TB in the deformed Mg-3Y. The inset in the figure is the corresponding fast Fourier transform image showing the  $\{10\bar{1}2\}$  twin-matrix orientation relationship. The STEM-EDS map using K lines signals of Mg and Y (Fig. 1(d)) for the same region as Fig. 1(c) shows the enrichment of Y along the  $\{10\bar{1}2\}$  TB.

Atomic-resolution HAADF-STEM images in Fig. 2 show the detailed microstructure of deformation-induced Y segregation in Mg-3Y at dislocations and along  $\{10\bar{1}2\}$  TBs. Fig. 2(a) along a  $\langle 1\bar{2}10 \rangle$  zone axis shows a low-angle tilt boundary formed by an array



**Fig. 1.** Grain orientation maps of the Mg-3Y sample (a) before compression and (b) after  $\sim 2\%$  plastic compressive strain, at room temperature, along the rolling direction. (c) ADF-STEM image of a  $\{10\bar{1}2\}$  twin boundary. Inset is the corresponding fast Fourier transform image showing the  $\{10\bar{1}2\}$  twin-matrix orientation relationship. (d) STEM-EDS of the same region as (a) showing the segregation of Y at the twin boundary.



**Fig. 2.** Y segregation at atomic resolution in the Mg-3Y after deformation at room temperature. (a) HAADF-STEM image of Y segregation at the tensile regions of  $\langle a \rangle$ -type dislocation cores along a low-angle prismatic tilt boundary. (b) STEM-EDS of the same region as (a). (c) HAADF-STEM image of Y segregation at a  $\{10\bar{1}2\}$  coherent twin boundary segment. The schematic image in (d) shows the atomic positions of Y-rich columns on the tensile sites along the  $\{10\bar{1}2\}$  coherent twin boundary. (e) HAADF-STEM image showing Y-rich clusters formed at a faceted  $\{10\bar{1}2\}$  twin boundary containing basal-prismatic facets. (f) Size distribution of Y-rich clusters on basal-prismatic facets.

of dislocations. The Burgers circuit for these dislocations yields a Burgers vector that appears to be  $1/2\langle 10\bar{1}0 \rangle$  which is most likely the projection of  $1/3\langle 11\bar{2}0 \rangle$ , the Burgers vector of the most common basal dislocations in Mg alloys [1–6]. Less than 10 layers of brighter atomic columns are observed on the side of basal dislocation cores that experience tensile strain, suggesting the segregation of a heavier element, i.e., Y, at the dislocation cores. The STEM-EDS map in Fig. 2(b) confirms Y segregation at the dislocation cores. While basal dislocations are shown here, we note that Y segregation may occur near other dislocations as well, including those whose Burgers vectors contain a  $\langle c \rangle$  component. Diffusion of Y atoms with larger metallic radius than Mg [39] towards

dislocations is thermodynamically driven by the volume misfit of the Y atoms and stress field created by the dislocations. This phenomenon is expected to hinder the motion of dislocations, which could influence the strength and texture evolution in Mg alloys.

High-resolution STEM analysis shows that the  $\{10\bar{1}2\}$  TBs in the RD compressed Mg-3Y often have serrated morphologies, containing both CTB segments and BP facets. Fig. 2(c) shows a typical  $\{10\bar{1}2\}$  CTB, with a single layer of alternating brighter and darker columns. The brighter columns along the  $\{10\bar{1}2\}$  CTB, which are Y-rich, are located on the sites with larger volumes than that in the perfect Mg crystal, while darker columns are at the adjacent sites with smaller volumes, as schematically illustrated in the figure in

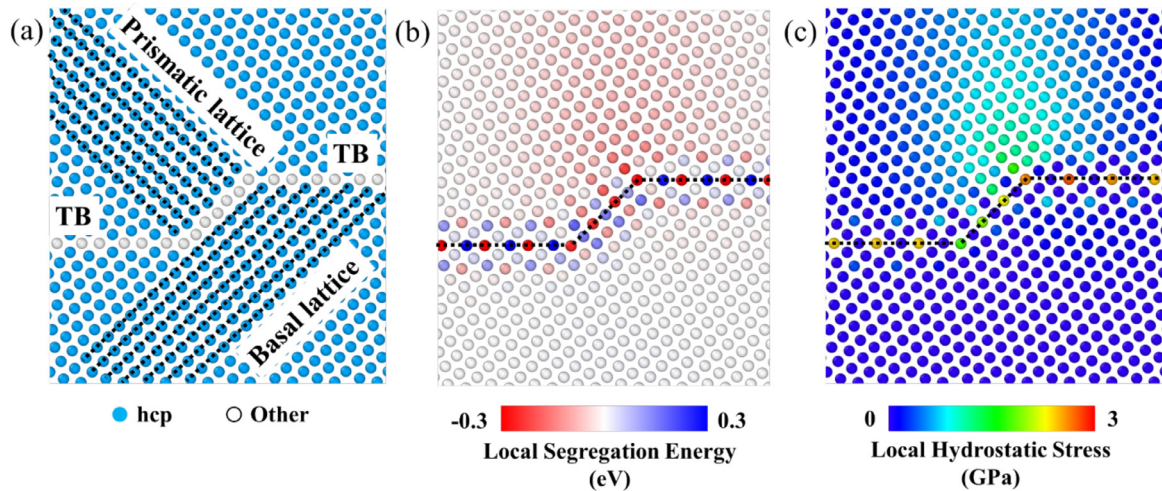


**Fig. 3.** (a) The atomic structure of the faceted twin boundary. Basal planes on both sides of the faceted twin boundary are marked using black dashed lines. (b) The distribution of Y segregation energy at sites near the interface, and (c) the distribution of atomic hydrostatic stress for the same region. In (b) and (c), the coherent twin boundaries and the basal-prismatic facet are marked using black dashed lines.

Fig. 2(d). Although such segregation has not been previously reported in Mg alloys deformed at room temperature, the presence of periodic Y segregation patterns along CTBs in the current study is consistent with that reported in deformed and annealed Mg-Gd [24], Mg-Zn [24], and Mg-Ag [28] alloys. Moreover, along a serrated  $\{10\bar{1}2\}$  TB shown in Fig. 2(e) that contains  $\{10\bar{1}2\}$  CTB segments (marked by red lines) and BP facets (marked by blue lines), Y-rich clusters were observed on the BP facets. The diameters of the Y-rich clusters on BP facets were measured from HAADF-STEM images taken along the  $\langle 11\bar{2}0 \rangle$  zone axis. The sizes of these clusters range from less than 1 nm to  $\sim 4$  nm, with an average size of 2 nm. Compared to segregation of solute atoms to CTBs, there are far fewer reports about segregation and clustering on BP facets. In the following, we assess the segregation tendency of a single Y atom to lattice sites near the BP facet with molecular statics and investigate the importance of this phenomenon on migration of a faceted TB using molecular dynamics (MD) simulation.

Atomistic simulations were conducted using the Large-scale Atomic/Molecular Massively Parallel Simulator (LAMMPS) package [40] and an embedded-atom method (EAM) potential developed by Sheng et al. [41]. An atomic snapshot of the simulation cell is shown in Fig. S2(d). A faceted TB with the length of a BP facet of approximately 1.63 nm was formed in the box, which is close to the experimental average of 2 nm (detailed information for generating the interface can be found in Section S2). To initiate TB motion, constant shear strain was applied globally by displacing all atoms in the simulation cell. Additional simulation details can be found in Section S3. An enlarged view of the faceted boundary is presented in Fig. 3(a). One Mg atom in the vicinity of the BP facet was replaced by one Y atom at a time, and the segregation energy,  $\Delta E_{seg}$ , was calculated as Eq 1:

$$\Delta E_{seg} = (E_{Twin}(Mg_{n-1}Y_1) - E_{Twin}(Mg_n)) - 1 \cdot (E_{Bulk}(Mg_{n-1}Y_1) - E_{Bulk}(Mg_n)) \quad (1)$$

where  $E_{Twin}(Mg_{n-1}Y_1)$  is the energy of a cell with the faceted TB and one segregated Y atom,  $E_{Twin}(Mg_n)$  is the energy of a cell with the faceted TB and without Y atoms,  $E_{Bulk}(Mg_{n-1}Y_1)$  is the energy of Mg single crystal with one Y atom, and  $E_{Bulk}(Mg_n)$  is the energy of pure Mg single crystal. A negative value of segregation energy indicates a preference for segregation, while a positive value predicts depletion. A comparison of our calculated segregation energy with reported density functional theory (DFT) calculations can be found in Section S4. According to Fig. 3(b), lattice sites that have the strongest preference for Y segregation are periodically patterned

along the CTBs and clustered adjacent to the BP facet, which agrees well with our HAADF-STEM results in Fig. 2(c and e).

To understand the origin of Y segregation on faceted  $\{10\bar{1}2\}$  TBs, the atomic hydrostatic stress of the same region is presented in Fig. 3(c). The magnitude of hydrostatic stress measures the degree of lattice distortion, with positive values indicating sites under tension. Obvious correlations between Fig. 3(b) and Fig. 3(c) are found: (1) the alternating sites on the CTBs that prefer Y segregation and depletion match exactly with those under tension and compression, respectively, and (2) a collection of sites near the BP facet that exhibit preference for Y segregation are also sites under apparent tension. These sites are under tension due to the lattice mismatch because the repeating unit of the basal lattice in Mg ( $\sqrt{3}a$ , where  $a$  is the  $\langle 11\bar{2}0 \rangle$  lattice parameter of Mg, with a value of 0.320 nm [42]) is slightly larger than that of the prismatic lattice ( $c$ , where  $c$  is the  $\langle 0001 \rangle$  lattice parameter of Mg, with a value of 0.520 nm [42]). Therefore, at a BP facet, the prismatic lattice remains under tension to match the basal lattice. Since the radius of Y (1.8 Å) is larger than that of Mg (1.6 Å) [39], the occupation of sites under tension by Y atoms can reduce the lattice distortion. We acknowledge that additional defects, such as dislocations, can be nucleated to relax the local stress along a BP facet, which may lead to different structures of Y segregation, but this is not explicitly treated here.

For Y to segregate to TBs, a sufficient mobility of the dopant species is necessary. The lattice diffusion coefficient for Y in Mg at room temperature is on the order of  $10^{-28}$  m<sup>2</sup>/s, as calculated by  $D = D_0 \exp(-Q/RT)$ , where  $R$  is the gas constant,  $T$  is the absolute temperature, and  $D_0 = 8 \times 10^{-6}$  m<sup>2</sup>/s and  $Q = 126.7$  kJ/mol [43]. In view of the low diffusivity, solute diffusion at room temperature could be enhanced by the dynamic interaction between solute atoms and crystallographic defects, i.e., TBs and dislocations, generated during deformation. As predicted by our simulation results, Y segregation at the extension sites along CTBs and adjacent to the BP facets is energetically favorable. Similarly, the strain field of dislocation cores could drive Y segregation to dislocations. The moving TBs and the gliding dislocations may act as sinks that accumulate and carry the solute atoms. When a basal  $\langle a \rangle$  dislocation interacts with a  $\{10\bar{1}2\}$  twin boundary, it will lead to the formation of a BP facet [36,44] and, at the same time, could transport solute atoms to the BP facet along the twin boundary. This is consistent with the STEM observation of Y enrichment at BP facets.

Recent studies have paid attention to the role of BP facets on the migration of  $\{10\bar{1}2\}$  TBs [31–36]. However, it is unclear how

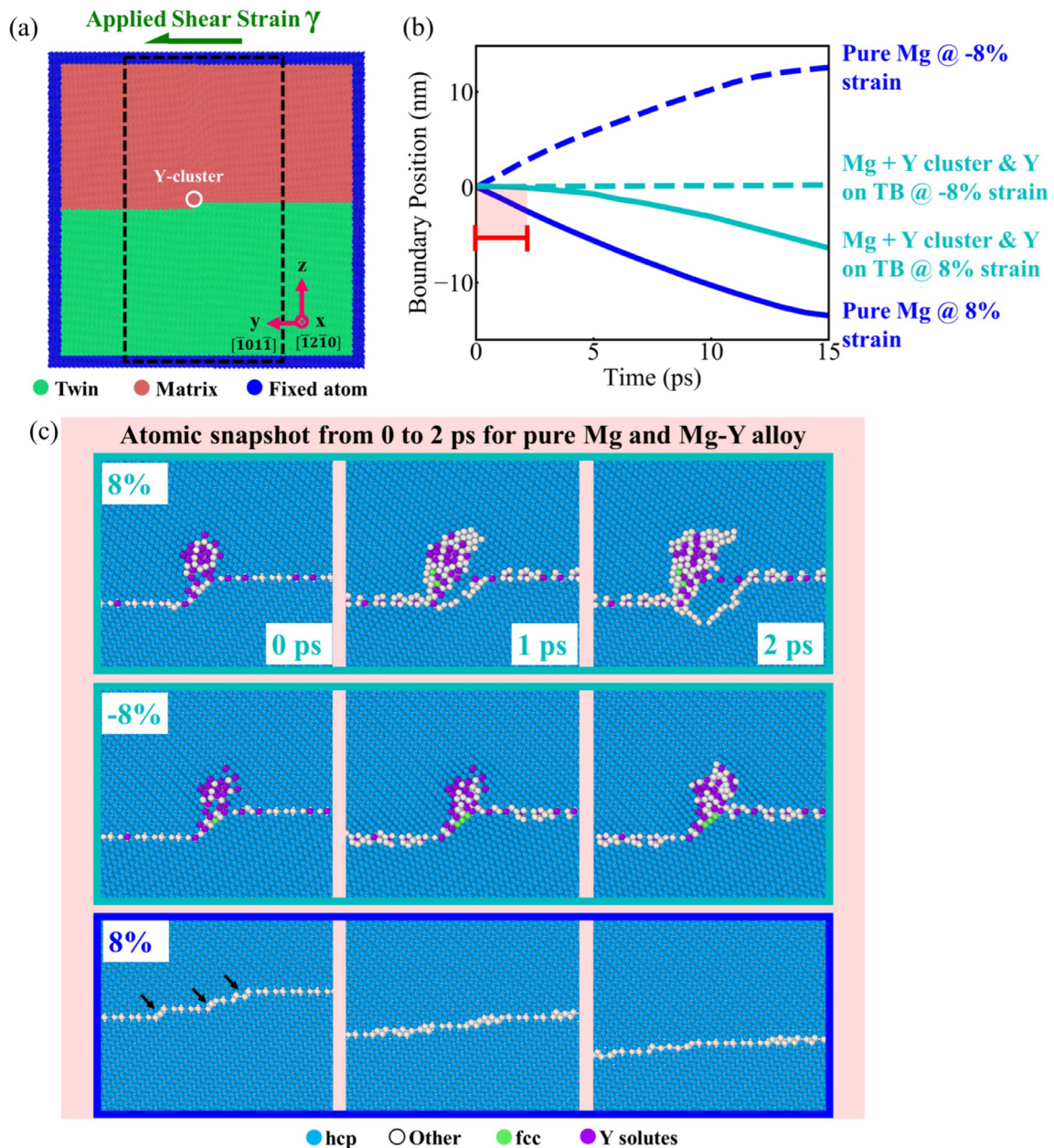


**Fig. 4.** (a) A schematic of the simulation cell used for shear-driven migration of the faceted twin boundary. Atoms colored in dark blue are fixed during simulation, while atoms in the mobile region are colored according to their lattice orientation. The green arrow on the top shows the direction of the positive shear strain. The rectangle shown by the black dashed line marks the part of the boundary used to calculate the average boundary position. (b) Boundary position versus time for pure Mg and Mg-Y alloys deformed at  $\pm 8\%$  shear strain. (c) Local atomic structure of the basal-prismatic facet from 0 to 2 ps for Mg-Y alloys deformed at  $\pm 8\%$  shear strain, and pure Mg deformed at 8% shear strain. Black arrows show the individual twinning dislocations formed from the basal-prismatic facet. (For interpretation of the references to colour in this figure legend, the reader is referred to the web version of this article.)

segregation of solute atoms at BP facets affects TB mobility. For this purpose, the migration of faceted TBs with and without the presence of Y atoms was compared using MD simulations. To represent the segregation phenomenon observed experimentally, multiple Y atoms were introduced into the simulation cell on lattice sites with larger volumes, which are the expanded sites on the CTBs and sites adjacent to the BP facet (see Section S5). A Y-rich cluster  $\sim 2.5$  nm in diameter was created at the BP facet, as shown in the schematic in Fig. 4(a). The boundary position under constant applied shear strain is plotted against time in Fig. 4(b). With the same shear strain, the faceted TB in Mg-Y moves slower than that in pure Mg, which can be attributed to a solute drag effect of Y atoms and clusters on the CTBs and BP facet. The segregated Y

atoms retard the motion of the faceted TB under both positive and negative shear strain, corresponding to more difficult twinning and detwinning and enhanced twinning-related hardening.

Moreover, unlike those for pure Mg, curves for the same amount of positive and negative shear strain are not symmetric about the initial position for Mg-Y, signaling that Y atoms lead to an anisotropy in boundary mobility. Fig. 4(c) shows the evolution of atomic structure around the BP facet in pure Mg and Mg-Y. Under -8% strain, although the CTBs start to become defected, the faceted TB in Mg-Y does not move during the simulation time. In contrast, under +8% strain, the TB unpins at the BP facet from the Y-rich cluster and starts to migrate downwards. For the downward migration, a minimum shear strain to unpin the TB from Y

solutes is ~6%, corresponding to a stress barrier ~1.43 GPa. In pure Mg, however, the BP facet is unstable and prefers to dissociate into three easy-glide twinning dislocations, a type of interfacial dislocation with both a dislocation character and a step height, which may explain why more highly serrated  $\{10\bar{1}2\}$  TBs are experimentally observed in Mg-Y alloys than those in pure Mg. These dissociated steps move and migrate quickly. Therefore, the segregated Y atoms on faceted TBs are expected to alter twinning-related hardening and plastic anisotropy, which affect the mechanical behavior and microstructural evolution of Mg alloys.

In summary, deformation-induced segregation of Y was observed in a Mg-Y solid solution alloy after deformation at room temperature, without subsequent annealing. Atomic resolution HAADF-STEM images show Y-rich columns at lattice dislocation cores, on the sites under tension along  $\{10\bar{1}2\}$  CTBs, and clustered adjacent to BP facets. Atomistic simulations indicate that Y segregation on CTBs and BP facets is mainly driven by the local lattice distortion. Such Y segregation and clustering can hinder TB motion and lead to anisotropic mobility of faceted TBs, which will affect twinning-related hardening and plastic anisotropy. Our results suggest that the mechanical behavior and microstructural evolution in Mg alloys can be strongly affected by deformation-induced solute segregation.

#### Declaration of Competing Interest

The authors declare that they have no known competing financial interests or personal relationships that could have appeared to influence the work reported in this paper.

#### Acknowledgements

The authors acknowledge financial support from the National Science Foundation (NSF) CMMI-1729829 (UCI), CMMI-1729887 (UCSB), and CMMI-1723539 (UC-Davis). We thank Dr. Sangbong Yi and colleagues at HZG in Germany for providing the Mg-Y alloy. The authors also acknowledge the use of facilities and instrumentation at the UC Irvine Materials Research Institute (IMRI) supported in part by the National Science Foundation Materials Research Science and Engineering Center program through the UC Irvine Center for Complex and Active Materials (DMR-2011967). XW would like to acknowledge Dr. Mingjie Xu for his help and discussion on STEM experiments and Ms. Katherine Acord for her help on compositional analysis.

#### Supplementary materials

Supplementary material associated with this article can be found, in the online version, at doi:10.1016/j.scriptamat.2021.114375.

#### References

- [1] P.G. Partridge, *Metall. Rev.* 12 (1967) 169–194.
- [2] S.R. Agnew, Ö. Duygulu, *Int. J. Plast.* 21 (2005) 1161–1193.
- [3] W.B. Hutchinson, M.R. Barnett, *Scr. Mater.* 63 (2010) 737–740.
- [4] S. Ando, M. Tsushida, H. Kitahara, *Mater. Sci. Forum* 706–709 (2012) 1122–1127.
- [5] D. Zhang, L. Jiang, X. Wang, I.J. Beyerlein, A.M. Minor, J.M. Schoenung, S. Mahajan, E.J. Lavernia, *J. Mater. Res.* 34 (2019) 1542–1554.
- [6] Z. Wu, W.A. Curtin, *Nature* 526 (2015) 62–67.
- [7] M.R. Barnett, *Mater. Sci. Eng. A* 464 (2007) 1–7.
- [8] M.R. Barnett, *Mater. Sci. Eng. A* 464 (2007) 8–16.
- [9] Y. Cui, Y. Li, Z. Wang, Q. Lei, Y. Koizumi, A. Chiba, *Int. J. Plast.* 99 (2017) 1–18.
- [10] S.R. Agnew, M.H. Yoo, C.N. Tomé, *Acta Mater.* 49 (2001) 4277–4289.
- [11] S. Miura, S. Imagawa, T. Toyoda, K. Ohkubo, T. Mohri, *Mater. Trans.* 49 (2008) 952–956.
- [12] Y. Chino, K. Sassa, M. Mabuchi, *Mater. Sci. Eng. A* 513–514 (2009) 394–400.
- [13] S. Sandlöbes, M. Friák, J. Neugebauer, D. Raabe, *Mater. Sci. Eng. A* 576 (2013) 61–68.
- [14] D. Zhang, H. Wen, M.A. Kumar, F. Chen, L. Zhang, I.J. Beyerlein, J.M. Schoenung, S. Mahajan, E.J. Lavernia, *Acta Mater.* 120 (2016) 75–85.
- [15] Z. Wu, R. Ahmad, B. Yin, S. Sandlöbes, W.A. Curtin, *Science* 359 (2018) 447–452.
- [16] Y. Chino, M. Kado, M. Mabuchi, *Acta Mater.* 56 (2008) 387–394.
- [17] Y. Chino, M. Kado, M. Mabuchi, *Mater. Sci. Eng. A* 494 (2008) 343–349.
- [18] J.A. Yasi, L.G. Hector, D.R. Trinkle, *Acta Mater.* 58 (2010) 5704–5713.
- [19] A. Tehranchi, B. Yin, W.A. Curtin, *Acta Mater.* 151 (2018) 56–66.
- [20] M. Ghazisaeidi, L.G. Hector, W.A. Curtin, *Acta Mater.* 80 (2014) 278–287.
- [21] A.H. Cottrell, B.A. Bilby, *Proc. Phys. Soc. A* 62 (1949) 49–62.
- [22] S.M. Zhu, J.F. Nie, *Scr. Mater.* 50 (2004) 51–55.
- [23] H. Aboulfadl, J. Degees, P. Choi, D. Raabe, *Acta Mater.* 86 (2015) 34–42.
- [24] J.F. Nie, Y.M. Zhu, J.Z. Liu, X.Y. Fang, *Science* 340 (2013) 957–960.
- [25] Y. Xin, X. Zhou, H. Chen, J.-F. Nie, H. Zhang, Y. Zhang, Q. Liu, *Mater. Sci. Eng. A* 594 (2014) 287–291.
- [26] Y.M. Zhu, S.W. Xu, J.F. Nie, *Acta Mater.* 143 (2018) 1–12.
- [27] X. Zhao, H. Chen, N. Wilson, Q. Liu, J.-F. Nie, *Nat. Commun.* 10 (2019) 3243.
- [28] X.F. Chen, L.R. Xiao, Z.G. Ding, W. Liu, Y.T. Zhu, X.L. Wu, *Scr. Mater.* 178 (2020) 193–197.
- [29] D.A. Basha, R. Sahara, H. Somekawa, J.M. Rosalie, A. Singh, K. Tsuchiya, *Scr. Mater.* 124 (2016) 169–173.
- [30] X.Y. Zhang, B. Li, X.L. Wu, Y.T. Zhu, Q. Ma, Q. Liu, P.T. Wang, M.F. Horstemeyer, *Scr. Mater.* 67 (2012) 862–865.
- [31] J. Wang, L. Liu, C.N. Tomé, S.X. Mao, S.K. Gong, *Mater. Res. Lett.* 1 (2013) 81–88.
- [32] K. Dang, S. Wang, M. Gong, R.J. McCabe, J. Wang, L. Capolungo, *Acta Mater.* 185 (2020) 119–128.
- [33] A. Serra, D.J. Bacon, *Philos. Mag.* A 73 (1996) 333–343.
- [34] A. Ostapovets, R. Gröger, *Model. Simul. Mater. Sci. Eng.* 22 (2014) 025015.
- [35] B. Xu, L. Capolungo, D. Rodney, *Scr. Mater.* 68 (2013) 901–904.
- [36] H. El Kadir, C.D. Barrett, J. Wang, C.N. Tomé, *Acta Mater.* 85 (2015) 354–361.
- [37] K. Hantzsche, J. Bohlen, J. Wendt, K.U. Kainer, S.B. Yi, D. Letzig, *Scripta Mater.* 63 (2010) 725–730.
- [38] S. Sandlöbes, S. Zaefferer, I. Schestakow, S. Yi, R. Gonzalez-Martinez, *Acta Mater.* 59 (2011) 429–439.
- [39] L. Pauling, *J. Am. Chem. Soc.* 69 (1947) 542–553.
- [40] S. Plimpton, *Fast Parallel Algorithms for Short-Range Molecular Dynamics*, Sandia National Labs., Albuquerque, NM (United States), 1993.
- [41] <https://sites.google.com/site/eampotentials/Home/MgY>.
- [42] R.S. Busk, *JOM* 2 (1950) 1460–1464.
- [43] W. Zhong, J.-C. Zhao, *Metall. Mater. Trans. A* 48 (2017) 5778–5782.
- [44] M. Gong, G. Liu, J. Wang, L. Capolungo, C.N. Tomé, *Acta Mater.* 155 (2018) 187–198.